Asymptotics for spherical particle motion in a spherically expanding flow.

V. V. Zakharov, S.L. Ivanovski, Jean-François Crifo, V. Della Corte, A. Rotundi, M. Fulle

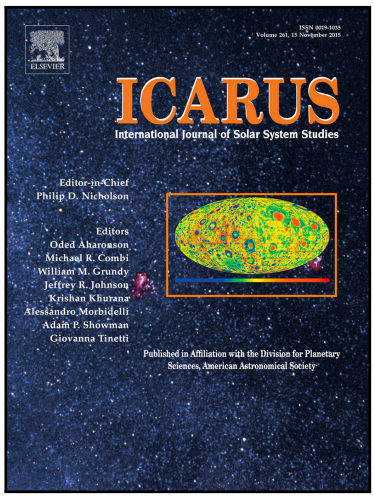

Asymptotics for spherical particle motion in a spherically expanding flow.

V.V. Zakharov, S.L. Ivanovski, J.-F. Crifo, V. Della Corte, A. Rotundi, M. Fulle

PII: S0019-1035(17)30843-6
DOI: 10.1016/j.icarus.2018.04.030
Reference: YICAR 12886

To appear in: *Icarus*

Received date: 20 December 2017
Revised date: 23 February 2018
Accepted date: 26 April 2018

Please cite this article as: V.V. Zakharov, S.L. Ivanovski, J.-F. Crifo, V. Della Corte, A. Rotundi, M. Fulle, Asymptotics for spherical particle motion in a spherically expanding flow., *Icarus* (2018), doi: 10.1016/j.icarus.2018.04.030

Highlights

- Asymptotics for spherical particle motion in a spherically expanding flow

Asymptotics for spherical particle motion in a spherically expanding flow.

V. V. Zakharov[a,*], S. L. Ivanovski[b,d], J.-F. Crifo[c], V. Della Corte[b,d], A. Rotundi[b,d], M. Fulle[e]

[a] *Laboratoire de Métérologie Dynamique, Université Pierre et Marie Curie, 4 place Jussieu, 75252 Paris, France*
[b] *INAF - Istituto di Astrofisica e Planetologia Spaziali, Area Ricerca Tor Vergata, Via Fosso del Cavaliere 100, 00133 Rome, Italy*
[c] *LATMOS, CNRS/UVSQ/IPSL, 11 boulevard d'Alembert, 78280 Guyancourt, France*
[d] *Università degli Studi di Napoli Parthenope, Dip. di Scienze e Tecnologie, CDN IC4, 80143 Naples, Italy*
[e] *INAF - Osservatorio Astronomico, Via Tiepolo 11, 34143, Trieste, Italy*

Abstract

In the context of an increasing number of complex multiparametric dust coma models it was found convenient to construct an elementary model with a minimum number of parameters selected to represent the key processes acting on the dust. The models outputs can be used as a reference evaluation of these processes with rough estimates of the resulting dust properties e.g. velocity.

The present work introduces three, universal, dimensionless parameters which characterize the dust motion in an expanding flow, and computes as a function of these parameters the dust terminal velocity, the time it takes to acquire it, and the distance at which it is acquired.

The motion of dust grains is presented as a system of dimensionless ordinary differential equations the solution of which depends upon the above mentioned three parameters. The numerical integration of this system was performed over a wide range of parameter space covering the whole range of physically possible conditions.

Precomputed results of dust terminal velocity, time and distance where it is reached are presented in dimensionless form. To obtain dimensional values for a particular case it is sufficient to perform algebraic operations.

Keywords: comets: general – dust dynamics – methods: numerical simulations

*Corresponding author
Email address: vladimir.zakharov@lmd.jussieu.fr (V. V. Zakharov)

1. Introduction

The study of dust-gas outflow from cometary nuclei has a long history and has now reached a remarkable degree of sophistication. The pioneering dust coma studies (Whipple (1951), Dobrovolskiy (1961), Dobrovolskiy (1966), Probstein (1969), Shulman (1972), Wallis (1982), Gombosi (1986)) tried to derive analytical expressions keeping as much as possible a meaningful physical description, but often using exceedingly crude simplifications (e.g. omitting of gravity and/or solar pressure, assuming constancy of gas expansion velocity etc.).

More recently, numerical models of much higher complexity for the description of dust dynamics in the cometary coma appeared (e.g. Crifo (2006), Rodionov et al. (2002)). These models either solve a system of differential equations describing the dust motion, or, perform a numerical simulation of the process. To predict the spatial and temporal distribution of physical variables (density, velocity etc.) in the coma, such models introduce a large number of governing parameters characterizing processes. Therefore the relative role of these processes is not easy to ascribe and relevant intercomparison of model results becomes difficult.

Our present work may look surprising. Following older models, we study the motion of a single spherical particle in a spherically expanding flow of an ideal perfect gas. However, contrary to previous models, we always keep in mind that, in all possible cases, the motion of the particle is governed by *at least three forces:* the aerodynamic drag, the nucleus gravity and the solar radiation pressure force. The aim of this study is to reveal the general properties of dust motion in an expanding flow and to reveal the relative influence of the three principal forces – drag, gravity and radiation pressure.

2. The model

The nucleus gravity and solar pressure force acting on a grain have simple classical expressions (see below) – as long as we assume the nucleus to be a homogeneous sphere.

The assessment of the aerodynamic drag force on the grain is more complex. It requires, first, computing the whole gas flow field. In general, the gas expansion from a spherical source into vacuum has three characteristic regions (see Lukianov and Khanlarov (2000)). The non-equilibrium near-surface layer (Knudsen layer), where initially non-equilibrium flow (due to the boundary conditions) relaxes to an equilibrium state, then a region of equilibrium flow, and finally once more a region

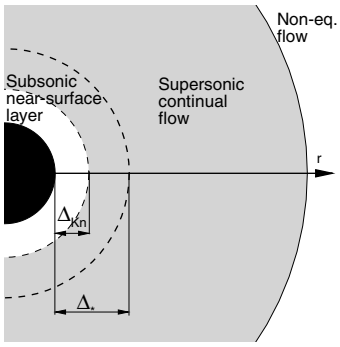

Figure 1: Flow structure in the source (Δ_*, Δ_{Kn} are the thickness of subsonic layer, non-equilibrium or Knudsen layer) .

of non-equilibrium flow resulting from the lack of intermolecular collisions. This scheme is shown in Fig. 1. The sizes of these three regions depend on the gas production of the source and may vary considerably. In the present study, we simplify the problem by assuming that the Knudsen layer is thin and the rest of the flow is in equilibrium. The gas flow is postulated as an adiabatic expansion of ideal perfect gas from a sonic spherical source, which means that on the nucleus surface we assume that the gas velocity is equal to the local sound velocity ($\sqrt{\gamma T_g k_b/m_g}$, where T_g is the gas temperature, m_g is the mass of the molecule, k_B is the Boltzmann constant and γ is the specific heat ratio). This assumption about sonic conditions on the initial surface is justified by the fact that the expanding flow into vacuum is always supersonic and therefore irrespective of the conditions of gas production, the sonic surface surrounds the nucleus.

This approximation has the merit of having a fully analytical solution (Landau and Lifshitz (1966)), which we use here.

In conclusion, the motion of a particle with invariable size and mass under the influence of aerodynamic drag, nucleus gravity, and solar pressure forces is described in our model by:

$$m_d \frac{dv_d}{dt} = \frac{(v_g - v_d)^2}{2} \rho_g \pi a^2 C_D(s, \frac{T_d}{T_g}) - \frac{G M_N m_d}{r^2} - \pi a^2 \frac{Q_{ef} c_\odot}{c r_h^2} \cos(z_\odot) \quad (1)$$

$$\frac{dr}{dt} = v_d \quad (2)$$

where a, m_d, v_d, T_d are the particle radius, mass, velocity and temperature, ρ_g, v_g are the gas density and velocity, M_N is the mass of the nucleus, G is the gravitational constant, Q_{ef} is the

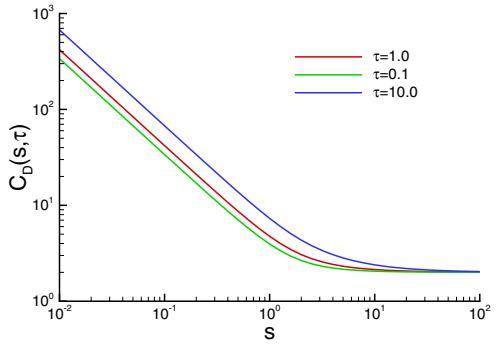

Figure 2: Variation of the drag coefficient C_D for $10^{-2} \leq s \leq 10^2$ and $\tau = T_d/T_g$=0.1, 1 and 100.

radiation pressure efficiency, c is the velocity of light, $c_\odot$ is the solar energy flux, $z_\odot$ is the solar zenith angle, r_h is the heliocentric distance (in AU), C_D is the drag coefficient, and r and t are radial distance and time, respectively. To use once more an existing analytical expression, we assume that the particle size a is everywhere much smaller than the mean free path of the gas molecules. The drag coefficient C_D is then given by the "free-molecular" expression for a spherical particle (see Bird (1994)):

$$C_D\left(s, \frac{T_d}{T_g}\right) = \frac{2s^2+1}{s^3\sqrt{\pi}} \exp(-s^2) + \frac{4s^4+4s^2-1}{2s^4} \mathrm{erf}(s) + \frac{2\sqrt{\pi}}{3s}\sqrt{\frac{T_d}{T_g}} \tag{3}$$

where $s = |\vec{v}_g - \vec{v}_d|/\sqrt{2T_g k_B/m_g}$ is a speed ratio. The variation of C_D in a wide range of s for three ratios of T_d/T_g is shown in Fig. 2.

In order to let chacteristic dimensionless parameters appear, let us rewrite the governing dust equations in dimensionless form, introducing the following dimensionless variables: $\theta = T_d/T_*$, $\tilde{v}_g = v_g/v_g^{max}$, $\tilde{v}_d = v_d/v_g^{max}$, $\tilde{r} = r/R_N$, $\tilde{t} = t/\Delta t$, $\tau = T_d/T_g$, $\tilde{\rho}_g = \rho_g/\rho_*$. Here $v_g^{max} = \sqrt{\gamma\frac{\gamma+1}{\gamma-1}\frac{k_b}{m_g}T_*}$ is the theoretical maximal velocity of gas expansion, ρ_* and T_* are the gas density and temperature on the sonic surface (i.e. on the surface of the nucleus) and $\Delta t = R_N/v_g^{max}$.

Then equations (1) and (2) can be rewritten as:

$$\frac{d\tilde{v}_d}{d\tilde{t}} = \tilde{\rho}_g(\tilde{v}_g - \tilde{v}_d)^2 C_D(s,\tau)\cdot \mathrm{Iv} - \mathrm{Fu}\cdot\frac{1}{\tilde{r}^2} - \mathrm{Ro}\cdot\cos(z_\odot) \tag{4}$$

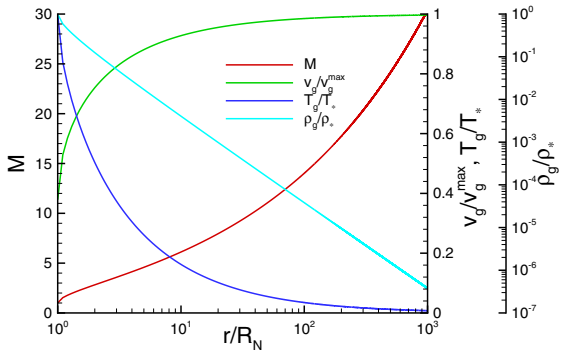

Figure 3: Radial distribution of M, v_g/v_g^{max}, T_g/T_*, ρ_g/ρ_* for γ=1.33.

$$\frac{d\tilde{r}}{d\tilde{t}} = \tilde{v}_d \tag{5}$$

Where $\tilde{v}_g$, $\tilde{r}$, τ and s in adiabatic spherical expansion (Landau and Lifshitz (1966)) are:

$$\tilde{v}_g = \left(\frac{(\gamma-1)M^2}{2+(\gamma-1)M^2}\right)^{1/2} \tag{6}$$

$$\tilde{r}^2 = \frac{1}{M}\left(\frac{2+(\gamma-1)M^2}{\gamma+1}\right)^{\frac{\gamma+1}{2(\gamma-1)}} \tag{7}$$

$$s = |\tilde{v}_g - \tilde{v}_d|\sqrt{\frac{\gamma}{\gamma-1}+\frac{\gamma}{2}M^2} \tag{8}$$

$$\tau = \theta\left(\frac{2+(\gamma-1)M^2}{\gamma+1}\right) \tag{9}$$

$$\tilde{\rho}_g = \left(\frac{2+(\gamma-1)M^2}{\gamma+1}\right)^{-\frac{1}{\gamma-1}} \tag{10}$$

Here $M = v_g/\sqrt{\gamma T_g k_b/m_g}$ is the Mach number. An example of the spatial distribution of gas parameters for γ=1.33 is given in Fig. 3.

The dimensionless parameters are:

$$\mathrm{Iv} = \frac{1}{2}\frac{\rho_*\sigma_d R_N}{m_d} = \frac{3Q_g m_g}{32R_N a\rho_d\pi\sqrt{T_*\gamma k_B/m_g}} \tag{11}$$

and

$$\mathrm{Fu} = \frac{GM_N}{R_N}\frac{1}{(v_g^{max})^2} \tag{12}$$

and

$$\mathrm{Ro} = \frac{1}{m_d(v_g^{max})^2} R_N \frac{\sigma_d Q_{ef} c_\odot}{c r_h^2} \tag{13}$$

Here Q_g is the total gas production rate, σ_d and ρ_d are the particle cross-section and specific density respectively.

We note that the theoretical maximum velocity of gas expansion could be expressed also in terms of a stagnation temperature T_0 and a heat capacity C_p as $v_g^{max} = \sqrt{2C_pT_0}$. In this way the gas velocity on the sonic surface is $v_* = \sqrt{2C_pT_0}\sqrt{\frac{\gamma-1}{\gamma+1}}$ and the gas production in [kg m^{-2} s^{-1}] is $q = \rho_* v_*$. Therefore we can rewrite Iv as:

$$\mathrm{Iv} = \sqrt{\frac{\gamma+1}{2(\gamma-1)}}\frac{3qR_N}{8\sqrt{C_pT_0}a\rho_d} \tag{14}$$

The second term in this equation is the reciprocal of a dimensionless similarity parameter characterizing the ability of a dust particle to adjust to the local gas velocity introduced in Probstein (1969).

As can be seen the three parameters have the following meaning:

1. Iv represents the ratio of the gas mass present in a flow tube with the cross section of the particle and a characteristic length, R_N, to the particle mass. This parameter characterizes the efficiency of entrainment of the particle within the gas flow (i.e. the ability of a dust particle to adjust to the gas velocity);
2. Fu represents the ratio of the comet surface gravitational potential to the flow thermodynamic potential (enthalpy, C_pT_0). This parameter characterizes the efficiency of gravitational attraction;
3. Ro represents the ratio of the specific work done by the solar pressure force on the characteristic length R_N to the flow thermodynamic potential. This parameter characterizes the contribution of solar radiation pressure.

In order to define Iv, Fu, Ro it is necessary to know: m_g, γ, Q_g (or ρ_*), T_*, R_N, M_N, a and ρ_d (or σ_d and m_d), Q_{ef} and r_h.

3. Results

The present study covers the range of Iv = 10^5–10^{-10}, Fu = 0.1–10^{-10}, Ro/Fu = 1.0–0.0 and $\gamma = 1.33$ and $\theta = 1$. For simplicity, we study only the case when $\cos(z_\odot)$=1 (i.e. sunward direction). The gas velocity is permanently increasing – initially rapidly and then quite slowly. For γ=1.33 it reaches 0.9 and 0.99 of v_g^{max} at $\tilde{r}$=6.4 and 185 correspondingly (see fig. 3). Therefore we limited the radial size of the computational domain to $\tilde{r} \leq 10^3$. For numerical integration of the system defined by equations (4) and (5) we used the Bulirsch-Stoer method (Press (1986)).

The condition that the grain could be lifted from the surface is:

$$\frac{\gamma - 1}{\gamma + 1} C_D(\sqrt{\gamma/2}, \theta) \cdot \mathrm{Iv} > \mathrm{Fu} + \mathrm{Ro} \tag{15}$$

For θ=1, γ=1.33 and Ro = 0 this condition is: 0.794 Iv > Fu.

If we neglect the solar pressure force (i.e. Ro = 0), the maximum liftable size a_{max} is:

$$a_{max} = \frac{3 Q_g m_g C_D(\sqrt{\gamma/2}, \theta) \sqrt{T_* \gamma k_B / m_g}}{32 \rho_d \pi M_N G} \tag{16}$$

and $a_{max} = 1.075 \cdot 10^{-2} Q_g \sqrt{T_* m_g}/(\rho_d M_N)$ for θ=1, γ=1.33.

3.1. Case when Ro = 0

Let us first study the case when the solar pressure force could be neglected (i.e. Ro = 0). The accelerating aerodynamic force decreases with the same rate as the decelerating gravity attraction and therefore if a particle is lifted from the surface then it is continuously and monotonously accelerating.

Fig. 4 shows the particle velocity $\tilde{v}_d$ and transit time $\tilde{t}$ at the distances $\tilde{r}$=10, 10^2 and 10^3 (the particle velocities at $\tilde{r} = 10^2$ and 10^3 are practically indistinguishable and therefore shown only for $\tilde{r} = 10^3$). For the maximum values of Iv the grain velocity at $\tilde{r} = 10^3$ and the gas maximal velocity are very close. For Iv > 1 the velocity of a particle at $\tilde{r} = 10^3$ is practically the same for any Fu < 1. For Iv < 1 the velocity of the particle is very sensitive to Fu and is considerably smaller then the gas velocity. This is intuitively correct from inspection of equation (14), which shows that Iv is proportional to q/a.

Though the gas and dust velocity permanently increase at large distance their acceleration is very small and therefore as a terminal velocity of the particle (v_d^{max}) we take v_d at $\tilde{r} = 10^3$. Fig. 5

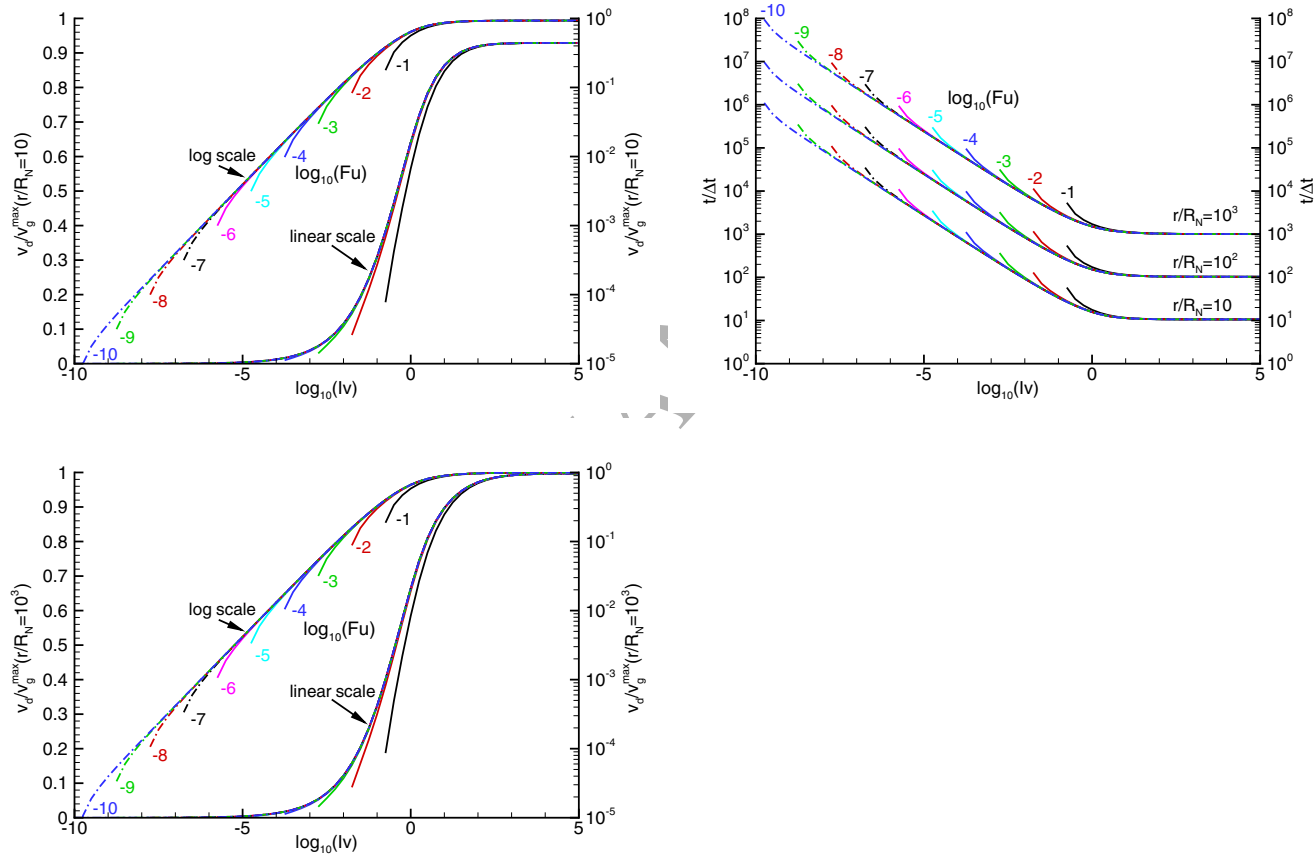

Figure 4: Particle velocity $\tilde{v}_d$ at $\tilde{r}$=10 (top left), particle velocity $\tilde{v}_d$ at $\tilde{r} = 10^3$ (bottom left) and transit time $\tilde{t}$ (top right) for $\gamma = 1.33$ and θ=1.0 (color numbers indicate the corresponding $\log_{10}$(Fu)).

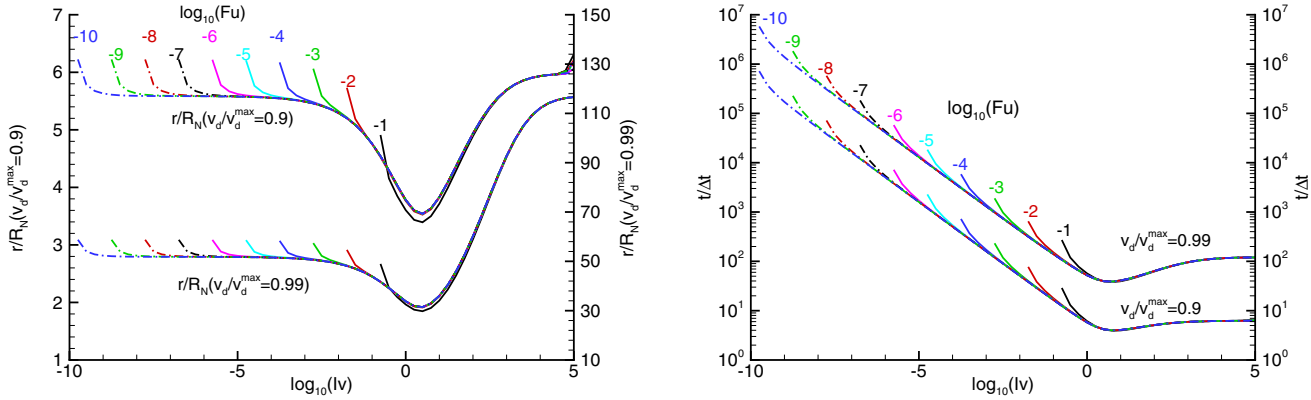

Figure 5: Distance (left) and time (right) when the particle reaches 0.9 and 0.99 of the terminal velocity for $\gamma = 1.33$ and θ=1.0 (color numbers indicate the corresponding $\log_{10}$(Fu)).

shows the distance and transit time when $\tilde{v}_d$ reaches 0.9 and 0.99 of the velocity at $\tilde{r} = 10^3$. For the maximum values of Iv the particle reaches 0.9 and 0.99 of the terminal velocity at $\tilde{r} = 6$ and 116.5, correspondingly. For Iv > 1 this distance does not depend on Fu (for Fu < 1) but for Iv < 1 it is very sensitive to Fu. It is interesting to note that the distance where the particle acceleration practically finishes (i.e. $v_d \approx$ const) has three characteristic ranges of Iv. For Iv $> 10^4$, it assymptotically approaches $\tilde{r} \approx 6$ for 0.9 of v_d^{max} (or $\tilde{r} \approx 116.5$ for $0.99 \cdot v_d^{max}$). For Iv $< 10^{-2}$ it assymptotically approaches $\tilde{r} \approx 5.6$ (or $\tilde{r} \approx 51.7$ for $0.99 \cdot v_d^{max}$). In the range $10^{-2} <$ Iv $< 10^4$ the variation of this distance is non-monotonic with minimum $\tilde{r} \approx 3.5$ (or $\tilde{r} \approx 30$ for $0.99 \cdot v_d^{max}$) at Iv ≈ 3.162.

In the above discussed cases the initial velocity of the particle was $\tilde{v}_d^0$=0. Now we study the cases when the particle has initial velocities from 0 up to 0.5. For a sonic source the gas velocity on the surface is: $\tilde{v}_* = \sqrt{\frac{\gamma-1}{\gamma+1}} = 0.376$, for γ=1.33. Note that we included also the case when the initial particle velocity is greater than the gas velocity at the surface (case $\tilde{v}_d^0 = 0.5$). Fig. 6 shows the particle velocity $\tilde{v}_d$ at the distances $\tilde{r}$=10 and 10^3 and it allows us to estimate the influence of the initial velocity at various Iv and Fu. For Iv > 1 a non-zero initial velocity is undetectable already at $\tilde{r} = 10$. But for Iv < 1, depending on Fu, the non-zero initial velocity may affect the particle velocity up to the external boundary of the region. The lower is Fu, the more noticeable is the influence of an initial velocity; this is particularly evident for the low values of the initial velocity.

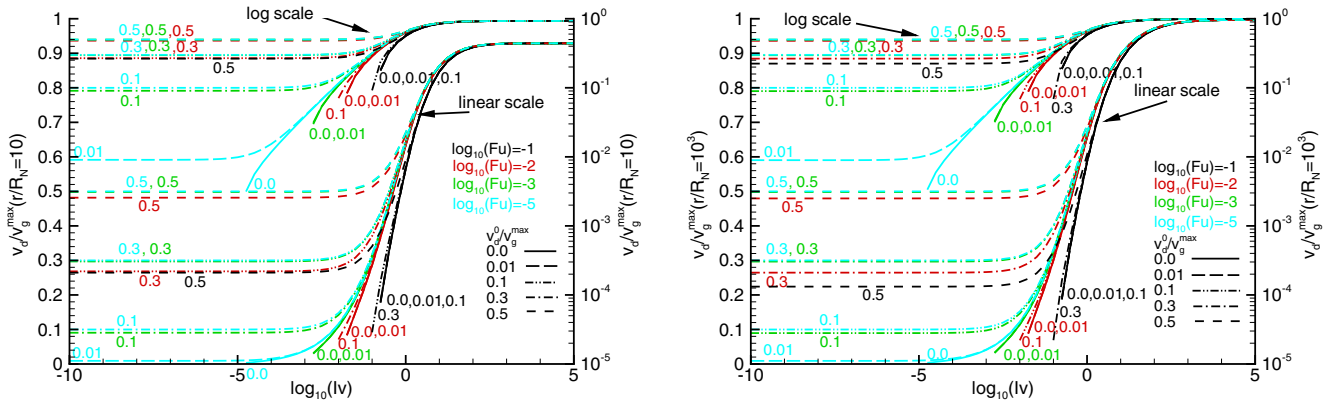

Figure 6: Velocity at radius $\tilde{r} = 10$ (left) and $\tilde{r} = 10^3$ (right) for different initial velocity $\tilde{v}_d^0$ for $\gamma = 1.33$ and θ=1.0. The color of the lines and labels corresponds to $\log_{10}$(Fu), the pattern of lines and values of labels correspond to $\tilde{v}_d^0$.

For example, at Iv $< 10^{-4}$ and Fu $< 10^{-4}$ the initial velocity $\tilde{v}_d^0 \geq 10^{-2}$ (and at Iv $< 10^{-2}$ and Fu $< 10^{-2}$ the initial velocity $\tilde{v}_d^0 \geq 0.1$) remains practically constant until exiting from the region. In the case Iv $< 10^{-2}$ and Fu $= 10^{-1}$ the particle with an initial very high velocity $\tilde{v}_d^0 = 0.5$ even decelerates.

3.2. Case when Ro > 0

Here we study only the case when $\cos(z_\odot) = 1$ (i.e. sunward direction) and Fu $\geq$ Ro. To simplify results representation, we express the solar pressure force as a fraction of the gravity force on the surface, which is equivalent to Ro/Fu. Since gas and dust velocity for $\tilde{r} > 6$ vary not much and the first term in eq.4 decrease as $\tilde{r}^{-2}$, the ratio Ro/Fu allows one to estimate the distance at which the solar pressure force starts to be sizeable.

The presence of non-zero solar pressure force, which does not decrease with distance, leads to a final deceleration of the particle motion. Fig. 7 shows the particle velocity $\tilde{v}_d$ at distances $\tilde{r}$=10 and 10^3, the transit time $\tilde{t}$ at distances $\tilde{r}$=10, 10^2 and 10^3, the particle maximal velocity, and the distance and time when it is reached. For this figure, if the particle did not start deceleration before $\tilde{r} = 10^3$, the particle velocity at the exit of the region is taken as the maximal velocity $\tilde{v}_d^{max}$.

At the distance $\tilde{r}$=10 there is no remarkable variation of velocity for $0 \leq$ Ro/Fu ≤ 0.1. But at the distance $\tilde{r}$=10^3 the distinction in velocity increases with increase of Fu. It should be noted

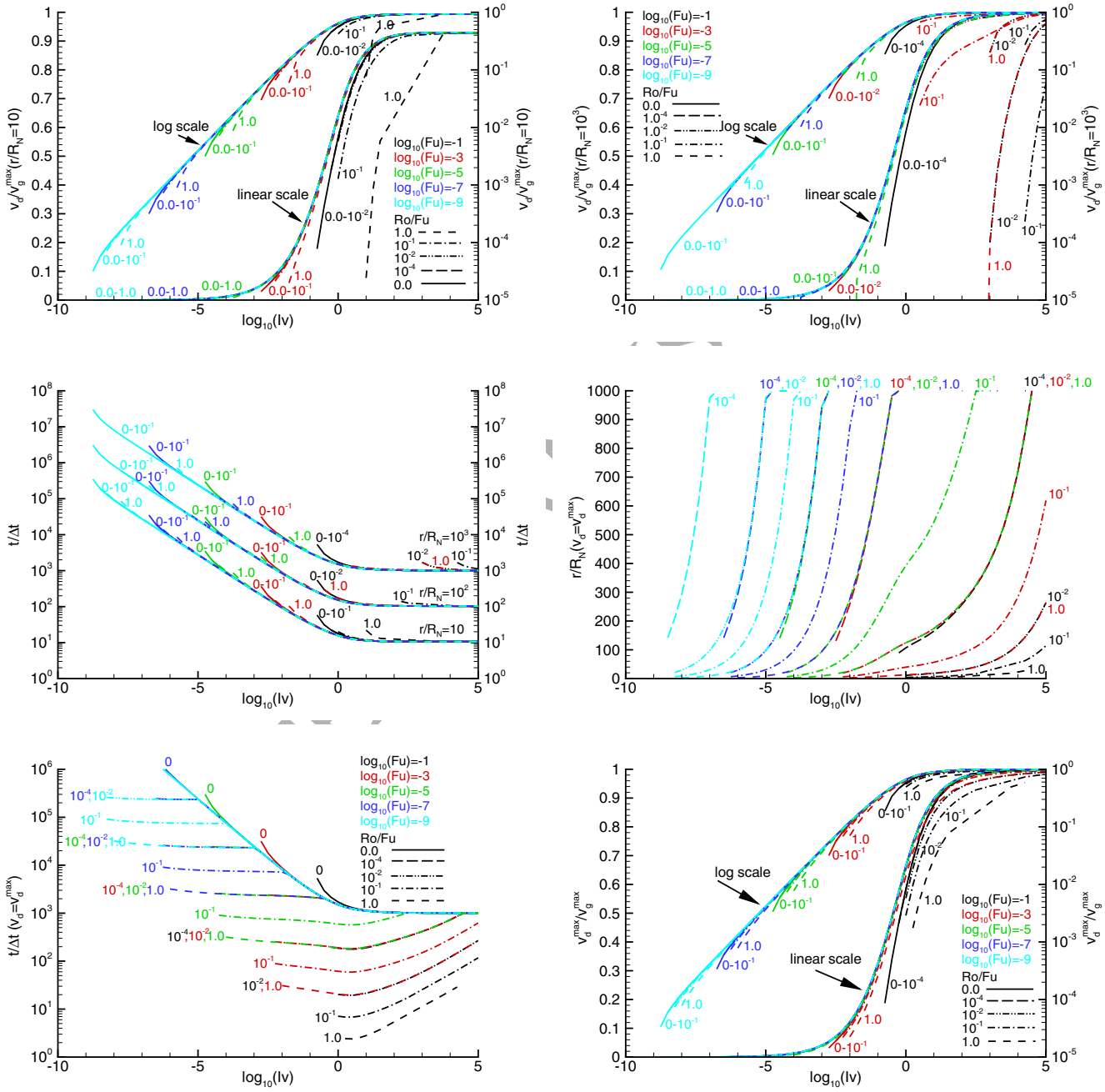

Figure 7: Particle velocity $\tilde{v}_d$ at $\tilde{r}$=10 (top left), particle velocity $\tilde{v}_d$ at $\tilde{r} = 10^3$ (top right), transit time $\tilde{t}$ (middle left), radius $\tilde{r}(\tilde{v}_d = \tilde{v}_d^{max})$ (middle left), transit time $\tilde{t}(\tilde{v}_d = \tilde{v}_d^{max})$ (bottom left) and maximum particle velocity $\tilde{v}_d^{max}$ (bottom right) for $\gamma = 1.33$, θ=1.0 and Ro > 0. The color of the lines and labels corresponds to $\log_{10}$(Fu), the pattern of lines and values of labels correspond to Ro/Fu.

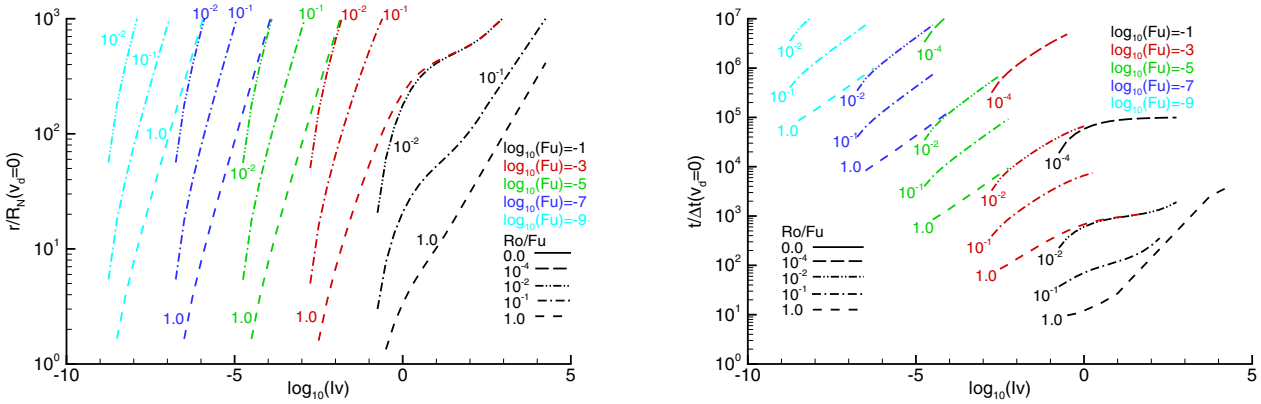

Figure 8: Radius $\tilde{r}(\tilde{v}_d = 0)$ (left) and transit time $\tilde{t}(\tilde{v}_d = 0)$ (right) for $\gamma = 1.33$ and θ=1.0. The color of the lines and labels corresponds to $\log_{10}$(Fu), the pattern of lines and values of labels correspond to Ro/Fu.

that since we use same ratios Ro/Fu in all cases, with increasing of Fu grows Ro as well. Fig. 7 shows the distance where $\tilde{v}_d^{max}$ is acquired (for Ro/Fu=0 this is $\tilde{r} = 10^3$) and the transit time required to achieve $\tilde{v}_d^{max}$. The transit time depends weakly on Iv < 1 for the given Fu and Ro. Note also that the transit times and the distances where $\tilde{v}_d^{max}$ is acquired are similar for the same Ro independently on Fu.

Fig. 8 shows the distance and time when the particle decelerates down to zero velocity. With growth of Iv the distance and transit time to the apex of the trajectory (where $\tilde{v}_d = 0$) become similar for the same Ro irrespective of Fu (since the value of Fu relative to Iv decreases).

4. Conclusion

The dust flow preserves typical general features regardless the particular coma model and the characteristics of the real cometary coma. We have presented an elementary model of particle motion in a spherically expanding flow parametrized by three dimensionless parameters (Iv, Fu, Ro). This model could be used as a reference model for the comparison of more sophisticated cometary dust coma models. It can also be used for rough estimations of the asymptotic behaviour of particle motion (terminal velocity, and distance and time when it is reached).

We intentionally skip the processes in the layer close to the surface since they are strongly

dependent on the local properties (irregularity and inhomogeneity of the nucleus). For the same reasons, in the case when dust grains have an initial velocity, we have omitted any discussion of the reasons how such an initial velocity might occur.

For evaluation of the aerodynamic force we used a spherically expanding flow of an ideal perfect gas. This idealized model of the flow practically never happens in real cometary atmosphere (non-equilibrium and rarefied) but it physically preserves integral properties of the real flow on a large scale correctly.

We would like to emphasize that the model, being oversimplified, cannot be used as a cometary coma model. But, based on the results presented, it is possible to estimate the relative influence of the main factors (aerodynamics, gravity, solar pressure, initial velocity) affecting every dust flow and reveal processes similarity.

OSIRIS data constrain the dust acceleration limited within six nuclear radii for a broad range of particle sizes (Gerig et al., 2018), in agreement with our model.

References

Bird, G.A., Molecular Gas Dynamics and the Direct Simulation of Gas Flows. Oxford, Clarendon Press, 1994.

Crifo, J.-F. 2006, Multidimensional physicochemical models of the near-nucleus coma: Present achievements and requested future developments, Advances in Space Research, 38, 19111922

Dobrovolskiy, O.V., 1961, Nonstationary process in comets and solar activity. Academy of Science of Tajik SSR, Dushanbe.

Dobrovolskiy, O.V., 1966, Komety (Moscow: Nauka).

Gerig, S.-B., Marschall, R., Thomas, N. et al. 2018, On deviations from free-radial outflow in the inner coma of comet 67P/Churyumov-Gerasimenko, Icarus (accepted for publication)

Gombosi, T.I., Nagy, A.F., Cravens, T.E. 1986, Dust and Neutral Gas Modeling of the Inner Atmospheres of Comets, Reviews of geophysics, vol. 24, No. 3, pp. 667-700

Landau, L.D., and Lifshitz, E.M., 1966, Fluid Mechanics, vol. 6, Pergamon Press, 1966.

Lukianov, G.A., and Khanlarov, Gr.O., 2000, Stationary expansion of water vapours from the sphere surface into vacuum. Thermophysics and Aeromechanics, vol.7, No.4, 489-498.

Markevich, M.Z., 1963, Bulletin of comets and meteros committee (in russian), N8, 11

Nakamura, R., Kitada, Y., Mukai, T. 1994, Gas drag forces on fractal aggregates, Planetary and Space Science, 42, N9, 721-726

Press, W.H., Teukolsky, S.A., Vetterling W.T. et Flannery, B.P. Numerical Recipes: The Art of Scientific Computing, Cambridge University Press, 1986.

Probstein, R.F., 1969, The dusty gas dynamics of comet heads. In Problems of Hydrodynamics and Continuum Mechanics, ed. M.A.Lavrent'ev (Philadelphia: SIAM), pp.568-583.

Rodionov,A.V., Crifo,J.-F., Szegő, K., Lagerros,J., Fulle, M., 2002 An advanced physical model of cometary activity, Planetary and Space Science, 50, 983–1024

Shulman, L.M., 1972, Dinamicka kometnikh atmosfer - neitralnii gaz, Naukova Dumka, Kiev.

Wallis, M.K., 1982, Dusty gas-dynamics in real comets, in Comets, L. L. Wilkening, (eds), 357-369,University of Arizona, Tucson.

Whipple, F., 1951, A comet model. II. Physical relations for comets and meteors, The Astrophysical Journal,113,464